Improving carbon coated TiO2 films with a TiCl4 treatment for photocatalytic water purification

ARTICLE

Improving carbon coated TiO_2 films with a $TiCl_4$ treatment for photocatalytic water purification

Gylen Odling, Aruna Ivaturi, Efthalia Chatzisymeon and Neil Robertson*[a]

Abstract: Using a simple thermal decomposition route, carbon-TiO_2 hybrid films have been synthesized from a catechol-TiO_2 surface complex. The coated films display enhanced visible region absorption, owing to the thin (~2 nm) layer of carbon encapsulating the TiO_2. While photocatalytically active under visible light alone, it is demonstrated that the activity of the carbon coated films can be improved further by a hydrolytic treatment with $TiCl_4$, leading to the introduction of small TiO_2 particles (5-10nm) and doping of chlorine into the structure. The combination of the carbon layer and $TiCl_4$ treatment gives increased photocatalytic performance for the photodegradation of dyes, phenolic pollutants and the reduction of toxic Cr(VI) to relatively benign Cr(III). In addition, the carbon coated films show improved bactericidal activity under UV irradiation, and hence have been successfully tested against the most common types of pollutant present in potential drinking waters.

Introduction

Removal of contamination from drinking water is quickly becoming one of the most pressing issues in the modern world[1,2]. Currently, it is estimated that water scarcity affects 40% of the global population, with this number expected to rise in coming years[3,4]. With a concurrent rise in the global population and increased industrialization of developing countries, contamination is becoming increasingly present in potable water sources[5]. The United Nations Global Goals for Sustainable Development include a division dedicated to clean water and sanitation, with a target to provide access to cheap, clean drinking water to all by 2030[6]. To this end, it is expected that water re-use and therefore purification will become a pressing issue to be solved in coming years[7]. In the removal of contamination from drinking water, there are three main targets that must be dealt with; organic molecules, inorganic metal ions and bacteria[8]. Current strategies to degrade these species typically involve the use of stoichiometric reagents[9,10] and/or the use of ultraviolet (UV) light[11–14]. While effective, these methods are ill-suited to many of the worst affected by water contamination, due to the high cost associated with continually acquiring purification reagents or the need for energy intensive UV lamps. Semiconductor photocatalysis has been shown in recent years to be effective in water purification[15–17]. Photo-oxidation of organic contamination[18–20], photo-oxidation or reduction of toxic metal ions to less toxic oxidation states[21–23], and the production of radicals that are highly effective in destroying bacteria have all been demonstrated using a variety of different semiconductors over recent years[24–26]. To date, the most studied semiconductor for this purpose is titanium dioxide (TiO_2)[27–29], which has gained much success due to its low cost, low toxicity and high stability. Much effort has been made to improve the efficiency of TiO_2 photocatalysts, including nanostructure modifications[30–33], band gap narrowing via doping[34–36], deposition of plasmonic metal nanoparticles[37–39], and the formation of composite materials with other inorganic semiconductors[40–42]. Organic-inorganic hybrids have also attracted significant attention, with materials such as graphitic carbon nitride[43–45], light harvesting polymers[46–48] or carbon quantum dots[49,50] being studied in composites with TiO_2 for photocatalytic applications. The coating of inorganic semiconductors with a carbon layer has been investigated in recent years as a method for improving photocatalytic efficiencies by decreasing charge recombination due to the intrinsic high conductivity of the carbon layer[51]. This effect has also been shown to increase the stability of some inorganic semiconductors under irradiation by reducing the likelihood for photo-induced charges to simply reduce or oxidise lattice ions[52,53], and provide a layer of chemical protection to the coated semiconductor.

Herein we describe the formation of a carbon coated TiO_2 film by pyrolytic treatment of a simply prepared TiO_2-catechol surface complex. We also describe a method by which the activity of this material can be improved by a simple hydrolysis of $TiCl_4$, resulting in the deposition of small (5-10nm) particles. This treatment has also been found to result in the doping of chlorine into the structure, resulting in a substantial increase in photocatalytic activity for the degradation of organic pollutants. These $TiCl_4$ treated composite materials also are found to exhibit good activity for the photoreduction of Cr(VI) to Cr(III), and bactericidal applications. As such, the prepared films are shown to be multi-functional, with photocatalytic activity against organic, inorganic and biological contamination. We believe that a single photocatalytic material immobilised in a film as described here with multiple functions is highly advantageous in providing a truly applicable material to real world contaminated water.

Results and Discussion

Film Preparation

It is well known that catechol binds strongly to the surface of TiO_2[54,55], forming a visible absorbing charge transfer complex indicating intimate contact between the resulting carbonaceous material and the TiO_2 surface. Subsequent hydrolysis of a solution

[a] Prof. Neil Robertson
School of Chemistry
University of Edinburgh
Joseph Black Building
David Brewster Road
Edinburgh
United Kingdom
EH9 3FJ
E-mail: n.robertson@ed.ac.uk

Supporting information and open data for this article is given via a link at the end of the document.

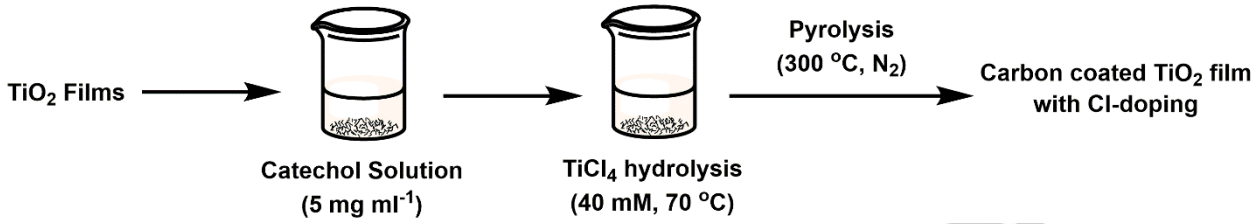

Figure 1. Preparation of the carbon coated and Cl-doped films.

of $TiCl_4$ in a similar manner to that which is typically used in the field of dye sensitized solar cells to deposit small (~5-10nm) particles onto the film surface[56] was found to not significantly affect the films appearance. Upon thermal treatment under N_2 the films were found to turn from the characteristic yellow colour of the surface complex to a light brown, indicating the decomposition of the organic catechol to carbon. The general synthetic procedure is given in Figure 1, where the initial TiO_2 film is formed by a doctor blading method (see experimental) giving a film which has previously been found to be 10-12 microns thick[57]. Hydrolysis of $TiCl_4$ to give TiO_2 is typically followed up with a thermal treatment step in air to give complete conversion to crystalline TiO_2. Here, by using relatively low temperatures and an inert atmosphere, some Cl remains in the lattice as a dopant. This represents a relatively simple method to introduce Cl as a dopant into TiO_2, which to the best of our knowledge has not been reported to date. Chlorine doped TiO_2 as a photocatalytic material is relatively unexplored, with only a few examples existing in the literature[58], where the Cl dopant is often paired with a co-dopant[59,60]. To explore the various components of the composite films, controls were prepared with only carbon coating (C-TiO_2), only $TiCl_4$ treatment with subsequent heating under N_2 (TiO_2-$TiCl_4$), and with both (C-$TiCl_4$-TiO_2).

UV-vis absorption spectroscopy

The as-prepared samples were all found to be semi-transparent, and therefore UV-vis transmission experiments were carried out to ascertain the films absorption characteristics (Figure 2).

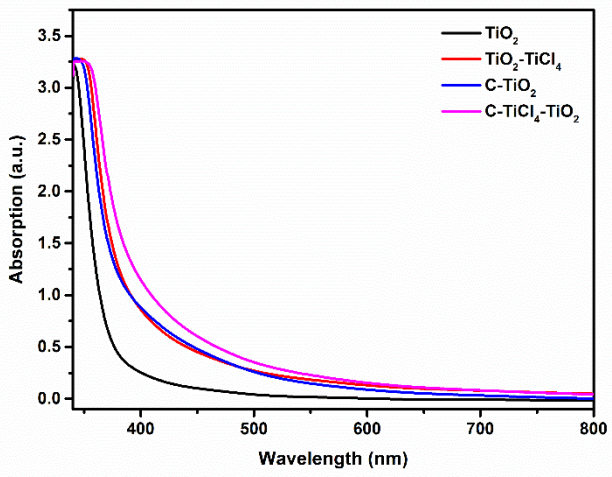

Figure 2. Uv-vis absorption characteristics of the photocatalyst films.

It was observed that each of the samples displayed superior visible light absorption when compared with pristine TiO_2. Of note is the absorption characteristics of TiO_2-$TiCl_4$, the visible light absorption of which is in keeping with the presence of Cl-doped TiO_2 being present. As reported by Wang et al[58], the extension of the absorption of TiO_2 into the visible by Cl doping typically leads to a broad absorption up to ~ 700 nm, accounting for the shift in absorption into the visible for TiO_2-$TiCl_4$.

X-ray diffraction

X-ray diffraction traces of the prepared materials are given in Figure 3.

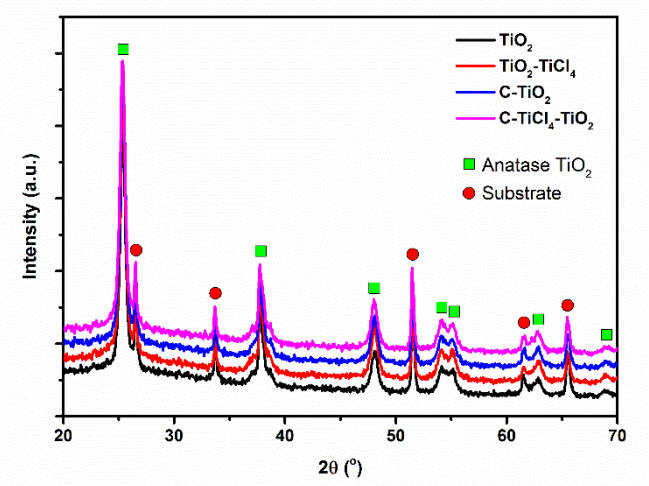

Figure 3. XRD traces of the prepared photocatalyst films.

Several peaks were found which match well with the reported 2θ values for anatase TiO_2 (JCPDS card #21-1272). The remaining peaks are identified as being due to the FTO glass substrate. Upon modification of the film, no new peaks were found, suggesting either amorphous materials and/or their presence being in too low a concentration to be detectable by XRD analysis. The crystallinity of the underlying TiO_2 film is found to be largely unaffected by the modifications made, keeping high crystallinity after modification. This is advantageous as good crystallinity has been noted to be important in ensuring rapid charge migration through the structure, resulting in improved photocatalytic efficiencies[61].

Electron microscopy

Scanning electron microscope (SEM) images of the pristine TiO_2 film surface revealed an interconnected porous network of

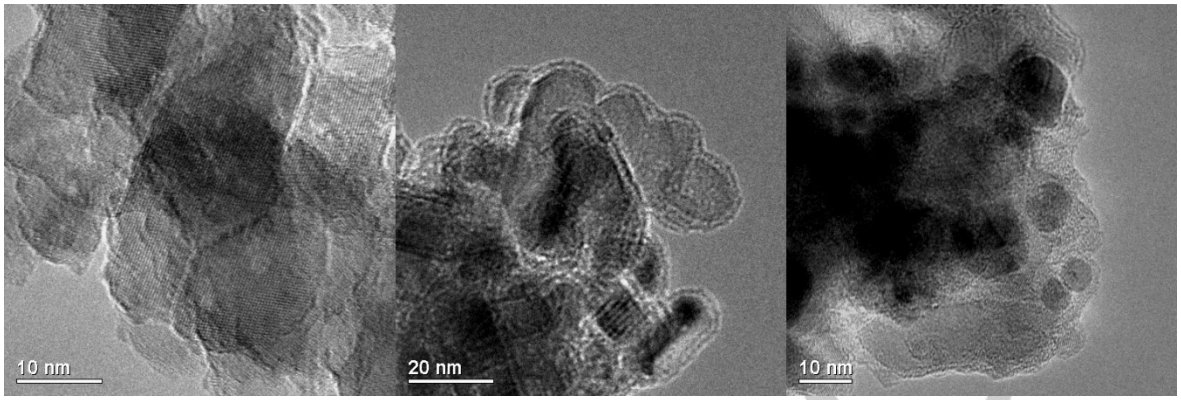

Figure 4. TEM images of TiO_2 (left), C-TiO_2 (mid) and C-$TiCl_4$-TiO_2 (right).

particles of approximately 20nm in size (Figure S1). However, no discernable differences were noted when the films were subjected to the carbon and/or the $TiCl_4$ treatments (Figure S2-4). To study the surface at greater magnification transmission electron microscope images were gathered (Figure 4). The unmodified TiO_2 particles were found to be well defined particles of around 20 nm in size. Clear lattice fringes of 0.35 nm were measured (Figure S5), which can be indexed to the [100] plane of anatase TiO_2. By contrast, images of the carbon coated sample (C-TiO_2) revealed that the lattice fringes were entirely obscured with amorphous material, with a layer of this material observed around the edges of the particles of around ~2 nm. This material we assign as a carbonaceous layer, formed by the pyrolytic decomposition of catechol. Images of C-$TiCl_4$-TiO_2 revealed smaller particles (5-10 nm) deposited across the surface, which originate from the hydrolysis of $TiCl_4$. It is noteworthy that, upon treatment with $TiCl_4$, the lattice fringes that were previously entirely obscured were now found to be at least partially visible (Figure S6), and the carbon layer was in places much thinner than in the C-TiO_2 sample. To prove the presence of Cl dopants in the particles originating from the hydrolysis of $TiCl_4$, TEM elemental mapping experiments were carried out upon C-$TiCl_4$-TiO_2 (Figure 5). The presence of Cl was clearly confirmed by the EDS mapping, showing the Cl present across the film. No distinct areas of high Cl concentration were noted, indicating that the doping of chlorine into the structure is applied equally across the entire structure, and is not confined to any particular area. Additional TEM images are given in the supporting information (Figure S7-9).

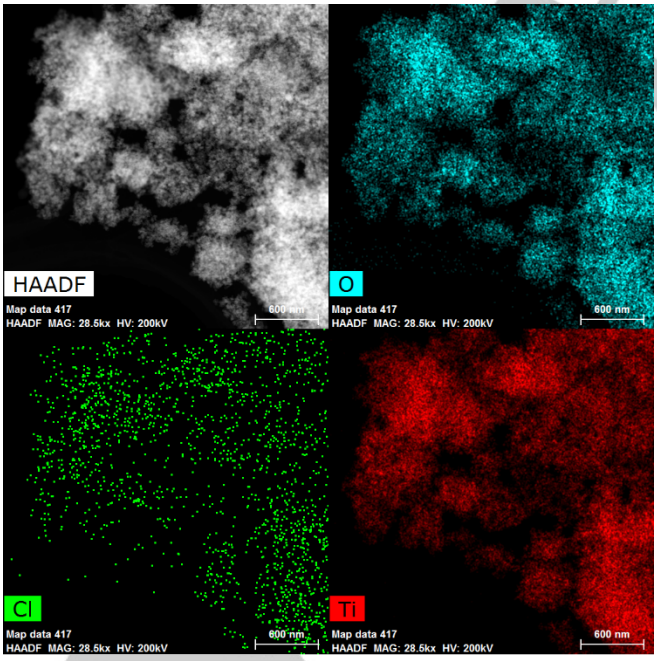

Figure 5. TEM-EDS maps of C-$TiCl_4$-TiO_2, showing the high angle annular dark field image (HAADF), oxygen (blue), chlorine (green) and titanium (red) maps of the area.

X-ray photoelectron spectroscopy

High resolution X-ray photoelectron spectroscopy (XPS) scans of the carbon and chlorine regions are given in Figure 6. Carbon is often found in XPS studies due to adventitious carbon introduced in the handling of samples. However, it was found that samples containing pyrolysed catechol had significantly higher peak intensities in the carbon region. Typically, carbon XPS peaks are split into the various chemical states of carbon. Fits of these various chemical states are given in Figure 6B. The lowest energy peak (~284 eV) has been previously assigned to sp_2 hybridised carbon in other carbon nanomaterials[62], which sees the greatest increase in intensity over the adventitious carbon in the unmodified sample. This is in keeping with the pyrolytic decomposition of catechol leaving the aromatic features of the catechol intact. The shoulder peak (~285 eV), typically assigned to sp_3 hybridised carbon, sees only a very small increase in intensity when compared to the pristine TiO_2 sample, indicating that the majority of the added carbon exists as planar sp_2 type carbon. The small peak at higher binding energy (~288 eV) is typical of carbon attached to oxygen[63], and sees little difference between C-TiO_2 and pristine TiO_2. High resolution XPS of the chlorine region (Figure 6C) revealed the presence of chlorine in the TiO_2-$TiCl_4$ and C-$TiCl_4$-TiO_2 samples, but not the pristine or C-TiO_2 samples. This confirms that the $TiCl_4$ hydrolysis and subsequent heat treatment under N_2 is not converting the deposited material entirely into TiO_2, and that some Cl is retained within the structure as a dopant. The two peaks for chlorine can be assigned to the $2p_{1/2}$ and $2p_{3/2}$ states of chlorine, which appear in positions in accordance with previously reported values for

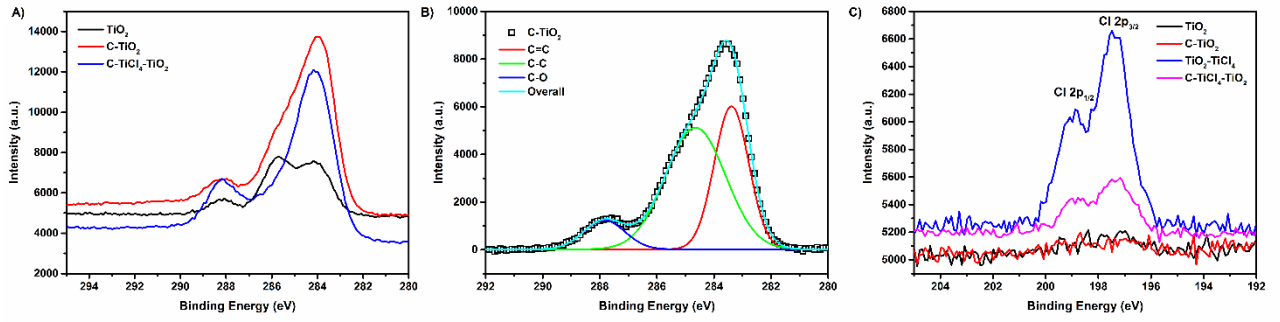

Figure 6. A) XPS scans of the carbon 1s region, B) peak fitting of the carbon peak for C-TiO_2 and C) XPS scans of the chlorine region.

chlorine doped materials[58,59]. No evidence for the introduction of nitrogen into the sample by the heating step under N_2 was found in the nitrogen region of the XPS (Figure S10), which discounts the presence of N-doped TiO_2, a common strategy for improving photocatalytic activity of TiO_2[64], in the samples which could have caused similar changes in the films' properties. Survey scans with peak assignments, as well as high resolution scans of the Ti and O regions are given in the supporting information (Figure S11-12).

Electrochemical Impedance Measurements

Electrochemical impedance has been proven to be an effective tool in probing the electronic structure of semiconducting films[65,66]. Impedance data for the prepared films was analysed according to the Mott-Schottky equation:

$$\frac{1}{C^2} = \frac{2}{e\varepsilon\varepsilon_o N_d}\left(E - E_{fb} - \frac{k_b}{T}\right)$$

Where ε is the dielectric constant of the material, ε_o is the permittivity of a vacuum, N_d describes the charge carrier density, E describes the applied potential, E_{fb} is the flat band potential and k_b/T describes thermal energy, which is considered to be small enough to be safely ignored. Plotting the inverse square of the capacitance against the applied potential therefore allows the flat band for the material to be easily read from the x-axis intercept, while the slope gives information about the charge carrier density and p- or n-type character of the material. The Mott-Schottky plots of the prepared films are given in Figure 7. All the films exhibit the positive slope associated with n-type materials, meaning that the dominant charge carriers in the films are electrons. Interestingly there appears to be little difference in the slopes of the plots, indicating that the charge carrier density in each film is approximately constant. Flat bands were determined using the fits shown in Figure 7, and are given in Table 1.

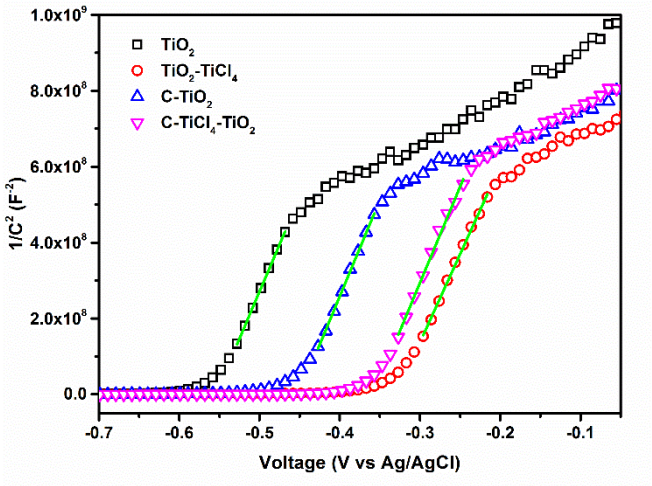

Figure 7. Mott-schottky analysis of the prepared films showing the linear regions used for fitting in green.

Table 1 Flat Band Potentials	
Sample	Flat Band Potential (V vs Ag/AgCl)
TiO_2	-0.555
TiO_2-$TiCl_4$	-0.330
C-TiO_2	-0.451
C-$TiCl_4$-TiO_2	-0.358

A clear shift is observed in the flat band potential upon going from pristine TiO_2 to C-TiO_2. This is to be expected, as carbon is well known to be a good electron accepting material[53], drawing electrons from electron rich TiO_2 and therefore shifting the flat band to more anodic potentials. The flat band potential of TiO_2-$TiCl_4$ is also found to have shifted anodically. Doping is often found to have pronounced effects upon the flat band of semiconducting materials[67], and a large anodic shift of the flat band is in keeping with dopant states being introduced just above the valence band maximum in a similar fashion to what has been observed in N-doped TiO_2 films[68]. This supports the presence of Cl doped TiO_2 being present upon $TiCl_4$ treatment. It is expected that if some lattice O ions are replaced with less electronegative Cl ions that dopant states would appear above the valence band maximum, and therefore the Fermi level of the semiconductor (and therefore the flat band) would be shifted anodically.

Photocatalytic Tests

The set up used for photocatalytic testing against methyl orange (MO), 4-chlorophenol (4-CP) and Cr(VI) is shown in Figure 8.

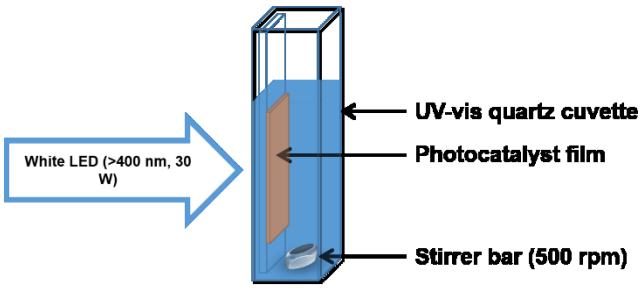

Figure 8. Diagram of the photocatalytic setup used in testing.

Prior to photocatalytic tests, each pollutant was stirred in this set up until no change in the absorption was observed (Figure S13-15). It is well known that photocatalytic degradation of pollutants in water follows pseudo 1st order rate kinetics[69], and therefore the rate constant can be obtained according to the following equation:

$$-\ln\left(\frac{C}{C_0}\right) = k_{app}t$$

Where C/C_0 is the fractional remaining concentration at a particular time, k_{app} is the pseudo 1st order rate constant in min^{-1} and t is time in minutes. The pseudo 1st order rate constant can therefore be obtained simply by reading the slope of a plot of $-\ln(C/C_0)$ against time. The rate plot for the prepared films for degradation of MO is shown in Figure 9.

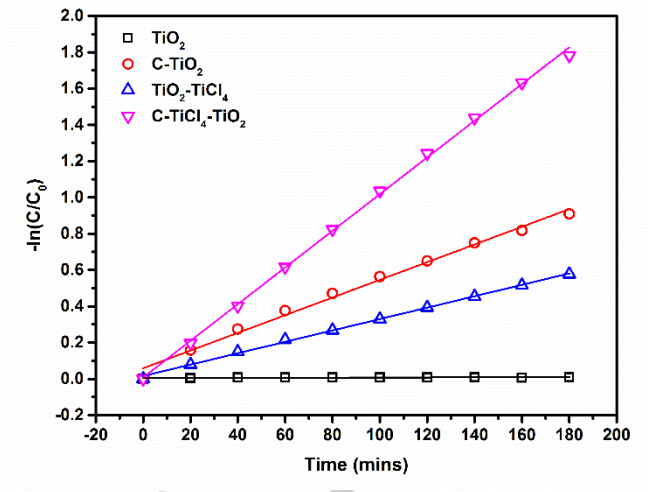

Figure 9. Pseudo 1st order rate plot for the prepared films upon MO under visible irradiation.

No degradation was observed for plain TiO_2, while TiO_2-$TiCl_4$, C-TiO_2 and C-$TiCl_4$-TiO_2 displayed increasingly rapid decolourisation of MO. As such it can be noted that the introduction of Cl doped TiO_2 improved the photocatalytic rate somewhat, as does the introduction of a carbon layer, while together they produce a highly effective photocatalyst. A summary of the photocatalytic activities of the samples is given in Table 2.

Table 2 MO photocatalytic degradation

Sample	Pseudo 1st order rate constant ($x10^{-3}$ min^{-1})
TiO_2	0.03
TiO_2-$TiCl_4$	3.14
C-TiO_2	4.87
C-$TiCl_4$-TiO_2	10.11

While dye decolourisation is widely applied as a preliminary measure of photocatalytic activity[70,71], we have previously found that it is not always a good metric for determining the effectiveness of a photocatalyst due to photosensitization of the semiconductor by the dye[72]. Excitation of an analyte dye in addition to the photocatalyst can increase rates significantly[73], and can make even plain TiO_2 appear to be active under visible only irradiation[74,75]. While not necessarily a problem if the end goal of a material is to degrade that specific dye, it leads to a photocatalyst which at best has activity which is specific to that particular dye, and could have vastly different activity against a different pollutant. Therefore, while an easy way of screening materials, the rates obtained using visible dyes should not be taken as being final. With this thought, further studies upon 4-CP, a colourless, UV absorbing phenolic pollutant, were carried out (Figure 10).

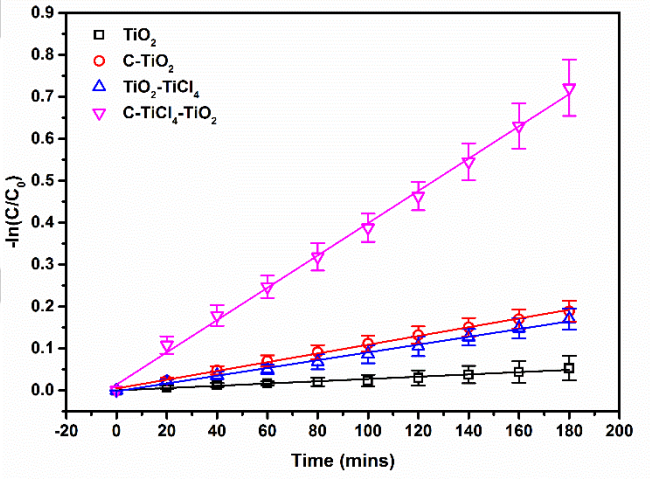

Figure 10. Pseudo 1st order rate plot of the photocatalytic degradation of 4-chlorophenol by the prepared films

The 1st order rate constants for 4-CP photodegradation are summarized in Table 3.

Table 3 4-CP photocatalytic degradation

Sample	Pseudo 1st order rate constant ($x10^{-3}$ min^{-1})
TiO_2	0.27 ± 0.17
TiO_2-$TiCl_4$	0.85 ± 0.13
C-TiO_2	1.00 ± 0.13
C-$TiCl_4$-TiO_2	3.86 ± 0.36

Immediately, a significant loss of activity is noted when comparing the degradation of 4-CP to MO. This can be ascribed to the loss of photosensitization that occurred using the visible dye MO. Otherwise a similar trend was seen in the photocatalytic activities,

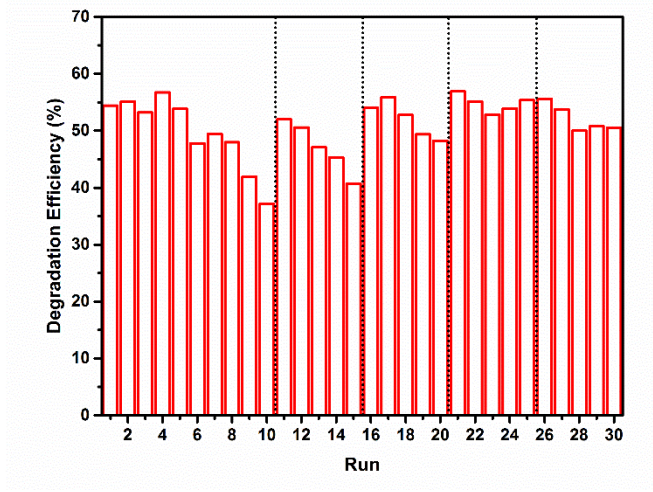

Figure 11. Recyclability test of C-$TiCl_4$-TiO_2 upon 4-chlorophenol. Each run is three hours. Dotted lines denote regeneration of the photocatalyst by heating under N2.

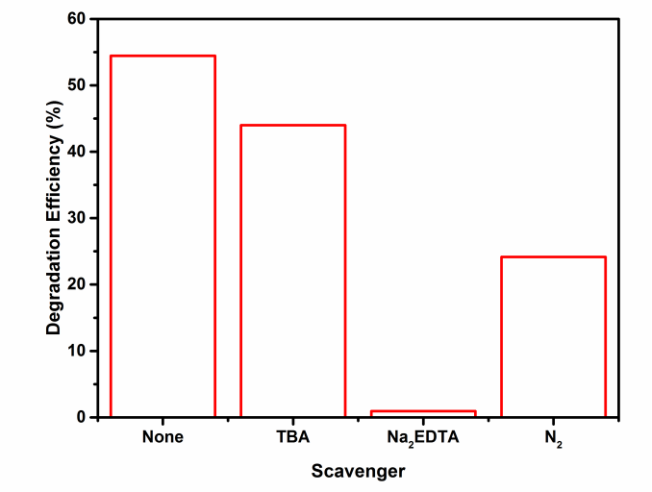

Figure 13. Scavenging tests upon the photocatalytic degradation of 4-chlorophenol.

although the TiO_2-$TiCl_4$ and C-TiO_2 films appeared to be within experimental error of one another, both had superior activity to pristine TiO_2. The C-$TiCl_4$-TiO_2 film produced significantly improved activity over all other samples, confirming that the combination of Cl-doping and a carbon layer is effective as a photocatalytic material. An advantage of the immobilization of the photocatalytic material as a film is the simplification of re-use. With a view to test this, repeated runs of 3 hours each were carried out upon the photocatalytic degradation of 4-CP (Figure 11). Degradation efficiency is determined as 1-C/C_0, the fractional quantity of 4-CP destroyed in 3 hours.

Initially, no losses of activity were noted, however towards 30 hours of irradiation (10 runs) the activity began to decrease. However, it was found that the photocatalyst could be regenerated by simply heating once again under nitrogen using the same method that was used in the synthesis (dotted lines in Figure 11). Using this method, the photocatalyst could be tested for 90 hours with no losses in activity. After 90 hours of testing, TEM studies revealed that the material in the film appeared to be largely unaffected by the irradiation/regeneration steps that had been applied, with the same ~10 nm particles and carbon layer upon larger ~20 nm particles being observed (Figure 12, SX).

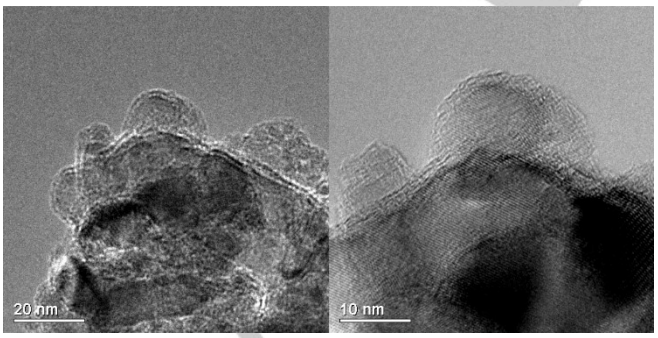

Figure 12. TEM images of C-$TiCl_4$-TiO_2 after 90 hours of use, showing the intact carbon layer and mix of large (20nm) and small (5-10nm) particles.

Introduction of a variety of different scavengers in high concentration has been used previously to effectively remove certain key species from the test, and the corresponding change in the degradation efficiency can be used to shed light upon the mechanism. Usually, scavenging experiments are carried out upon dye solutions[76,77]. However, as discussed previously, we believe this to be unreliable, as photosensitization can lead to the production of reactive species which would not occur in the photocatalytic degradation of different analytes, once again making the test an unreliable method to determine the important reactive species generated. Therefore, scavenging tests upon C-$TiCl_4$-TiO_2 were carried out using the photocatalytic degradation of 4-CP (Figure 13).

In this study, tert-butyl alcohol (TBA) was used as a scavenger of hydroxyl radicals, disodium EDTA was used to scavenge photogenerated holes and continuous degassing using N_2 was used to exclude O_2 from the solution, hindering the reduction of O_2 to the superoxide ion[78,79]. It was found that hydroxyl radicals play a minor role in the degradation of 4-CP, with a small decrease in the degradation caused by addition of TBA. The main oxidizing species however appears to be photogenerated holes, with addition of disodium EDTA causing almost complete loss of activity. The removal of O_2 from the 4-CP solution causes a partial drop in activity, indicating that electron transfer to O_2 to form superoxide is indeed important, which supports the formation of hydroxyl radicals which may be accessed via the superoxide ion[15].

In addition to organic pollution, heavy metal contamination is becoming increasingly common in urban industrialised water sources. Soluble chromium (VI) is a typical toxic metal contaminant resulting from a variety of industrial processes[80], which can be remediated by reduction to less toxic Cr(III). The photocatalytic reduction of Cr(VI) using C-$TiCl_4$-TiO_2 with phenol as a sacrificial electron donor is shown in Figure 15.

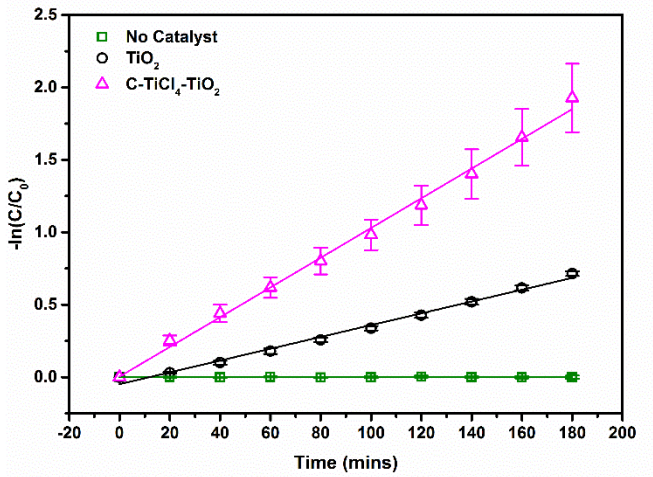

Figure 15. Pseudo 1st order rate plot of the photocatalytic reduction of Cr(VI) under visible light.

Once again C-$TiCl_4$-TiO_2 proved a superior photocatalyst to pristine TiO_2, the rate constants for Cr(VI) reduction are given in Table 4.

Table 4 Cr(VI) photocatalytic reduction

Sample	Pseudo 1st order rate constant (min^{-1})
No catalyst	0.00(5) ± 0.06
TiO_2	4.03 ± 0.08
C-$TiCl_4$-TiO_2	10.35 ± 1.15

Interestingly, TiO_2 alone gave some activity, most likely owing to photosensitization of the film by the chromium(VI) source, which has a pale yellow colour in aqueous solution. Solutions used in Cr(VI) photoreduction tests are typically acidified, which has been suggest to be due to the consumption of H^+ during the reduction[22] as follows:

$$Cr_2O_7^{2-} + 14H^+ + 6e_{cb}^- \rightarrow 2Cr^{3+} + 7H_2O$$

The low pHs used in this type of test are often too low to be used with many visible light active semiconductors such as sulfides, which are unstable in highly acidic solutions. Here, the highly stable carbonaceous material allows use of low pH and visible light irradiation, proving the applicability of this type of system for Cr(VI) photoreduction.

On this basis of the photocatalytic action for Cr(VI) and the scavenger tests described previously, the mechanism of action can be determined, and is represented in Figure 14.

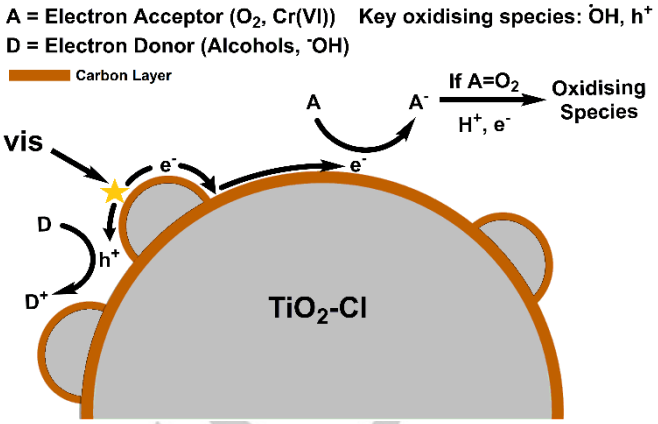

Figure 14. Proposed mechanism of photocatalytic action

Bactericidal activity

Escherichia coli (E. coli) are commonly used as a marker for bacterial content in contaminated of water[81]. Of the UV radiation reaching the earth surface, more than 95 % consists of longer wavelength UV-A component. Thus, in the present study the bactericidal activity of the TiO_2 and C-$TiCl_4$-TiO_2 samples were studied using the standard *E. coli* strain under UV-A exposure. To determine the relationship between UV-A light intensity and efficiency of photocatalytic inactivation, the disinfection kinetic constants were calculated using the classic disinfection model of Chick-Watson equation[82], shown as follows:

$$log\frac{N}{N_0} = -kt$$

where N/N_0 is the fraction remaining bacterial concentration at a particular time, k' is the disinfection kinetic constant, and t is the contact time. Due to the simplicity of this log-linear equation corresponding pseudo-first order kinetics, this model has been widely used to compare the efficiency of photocatalytic inactivation through the values of disinfection rate constant, k', where higher k' means better disinfection effectiveness. Figure 16 shows the linear fitted plots of the photocatalytic disinfection kinetics as per Chick-Watson model. Inset shows the digital photograph of the TiO_2 and C-$TiCl_4$-TiO_2 samples (3.5 × 3.5 cm^2) analysed for this study. The *E. coli* disinfection rate constant for C-$TiCl_4$-TiO_2 sample (k = 4.31×10^2 ± 0.36×10^2 min^{-1}) was observed to be nearly twice that of the pristine TiO_2 (k' = 2.65×10^2 ± 0.24×10^2 min^{-1}). Figure 17 shows the digital photographs of the Agar plates cultured with water samples spiked with *E coli* with the photcatalyst (TiO_2 and C-$TiCl_4$-TiO_2 samples) after (a) 120 minutes (b) 150 minutes and (c) 180 minutes of UV exposure. Clearly, the C-$TiCl_4$-TiO_2 samples show an enhanced bactericidal activity with total inactivation of *E. coli* observed after 3 hours of UV-A illumination as compared to the pristine TiO_2 sample. TiO_2 and carbon modified TiO_2 including nanocarbon/TiO_2 composite, multi-walled carbon nanotubes coated by TiO_2, TiO_2/carbon nanotubes composites etc have been widely tested for photocatalytic bactericidal activity[83–86]. The prevalent mechanism

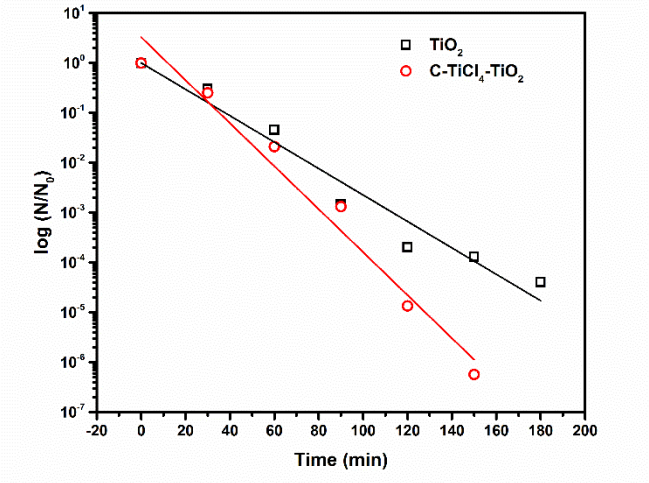

Figure 16. Linear fitted plots of the photocatalytic disinfection kinetics as per Chick-Watson model.

for the photocatalytic bactericidal activity of *E. coli* consists of oxidative damage of the cell wall and cell membrane and alterations of the internal DNA molecules.

Conclusions

C-$TiCl_4$-TiO_2 has been demonstrated as a versatile photocatalyst for environmental water remediation. It has been shown that using simple processing techniques both chlorine doping and thin carbonaceous layers may be deposited upon TiO_2 films. Together these two modifications are found to produce a very effective photocatalyst for the degradation of dyes, colourless pollutants, the photoreduction of chromium(VI) and the killing of bacteria. Such a comprehensive studie of a single material against all of these pollutant types is rarely found in the literature, but is important if photocatalytic materials are to be applied beyond the laboratory. The films also display good re-useability, being able to be regenerated and continually used for 90 hours without significant losses of activity. We believe that this combination of high activity, good re-useability and versatility of activity towards an example of each type of pollutant present in water sources demonstrates that this material is a prominent candidate for real world water purification.

Experimental Section

Film preparation:

FTO glass substrates were cut into 2cm x 2cm squares before being ultrasonically cleaned in a solution of detergent (Decon 90, ~5% in tap water) for 15 minutes. The substrates were then rinsed with tap water, deionised water and finally ethanol. Titania paste (Dyesol 18-NRT) was then doctor bladed in 1 cm x 2 cm strips onto the surface of the FTO using scotch tape (3M) as a spacer before heating to 510 °C in stages on a controlled hotplate to remove the organic templates, leaving a highly porous TiO_2 film. The temperature profile of the heating regime was as follows: 325 °C for 5 minutes, 375 °C for 5 minutes, 425 °C for 5 minutes, 475 °C for 10 minutes, 510 °C for 10 minutes. The heating ramp rate between each stage was 10 °C min^{-1} apart from the final stage where it slowed to 5 °C min^{-1}. The sintered TiO_2 films were then allowed to cool gradually on the hotplate to room temperature. Narrower (0.9 cm x 2 cm) films were also fabricated in the same way for photocatalytic degradation of methyl orange, 4-chlorophenol and Cr(VI) reduction. Wider films (3.5 cm x 3.5 cm) were also fabricated for the bactericidal testing studies.

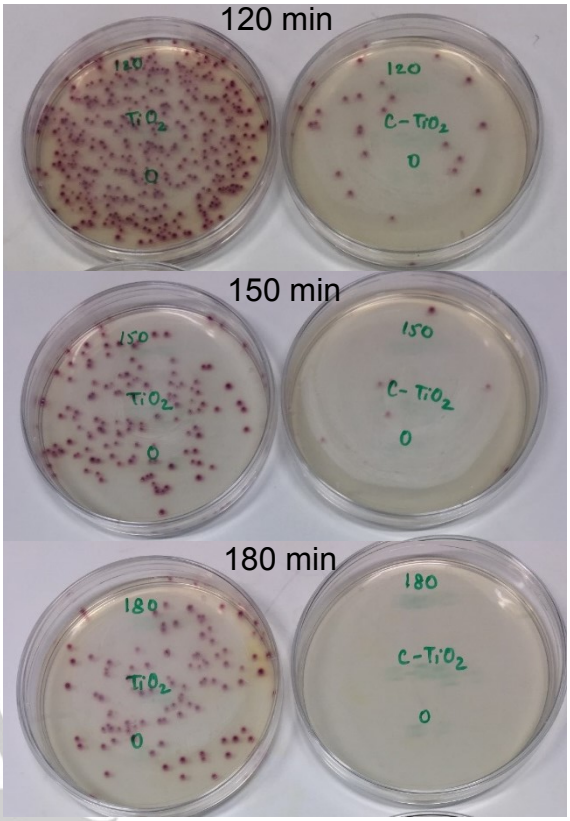

Figure 17. Digital photographs of the Agar plates cultured with water samples spiked with E. coli with the photcatalyst (Left hand side TiO_2 and right hand side C-$TiCl_4$-TiO_2 samples) after (a) 120 minutes (b) 150 minutes and (c) 180 minutes of UV-A exposure.

Sensitisation:

Films were dipped into catechol (5 mg/ml) for 30 minutes during which time the films became yellow in colour. The films were then rinsed thoroughly with de-ionised water before submerging in a solution of titanium tetrachloride (40 mM) and heating at 65 °C for 30 minutes. Films were washed thoroughly once again with deionised water and allowed to air dry before heating under N_2 (10 minutes at 200 °C, 30 minutes at 300 °C), during which time the films turned from yellow to brown, indicating the thermal decomposition of the catechol-TiO_2 surface complex.

Characterisation:

X-ray diffraction data were acquired on a Bruker D2 phaser model diffractometer using monochromated CuKα radiation. UV-visible absorption of the films was measured using a JASCO V-670 spectrophotometer. XPS scans were carried out using a Kratos Analytical AXIS Nova instrument with monochromated 1486.6 eV Al Kα irradiation. Transmission electron microscope (TEM) images were obtained using a Jeol JEM-2011 TEM operated with an accelerating voltage of 200 kV. TEM elemental mapping was acquired on a FEI Titan Themis electron microscope using a Super-X high sensitivity windowless EDX detector. SEM images were collected using a Carl Zeiss SIGMA HD VP Field Emission SEM, operated in InLens mode with a 10 kV accelerating voltage. Mott-Schottky analyses were performed using an Autolab PGSTAT30 with FRA software to control a standard three electrode setup. Ag/AgCl reference electrode and Pt wire counter electrode were used, with the film constituting the working electrode. The electrolyte used was 0.1 M Na_2SO_4 and the frequency used was 100 Hz. In all cases where a result is accompanied by an error range, the error has been calculated by three measurements on three separately prepared samples.

Photocatalytic testing:

Narrow films (0.9 cm x 2 cm) were submerged into a solution of methyl orange (2 ml, $4.6x10^{-5}$ molar) in a quartz cuvette. The films were stirred in the dark for up to 30 minutes to establish an adsorption equilibrium, determined as the point at which no further change to the absorbance of the solution occurred, and then irradiated with a white LED (30 W applied power) fitted with a UV filter (>400 nm, Thorlabs). The decolourisation of methyl orange was followed by measuring the absorption at 463 nm at regular time intervals using a JASCO V-670 spectrophotometer. The degradation of 4-chlorophenol was measured in the same way, using 4-chlorophenol of 156 µmolar concentration followed using the peak at 280 nm. In the assessment of the recyclability of the films, a single measurement after 3 hours irradiation was taken to calculate the degradation efficiency, between runs the film was washed with deionised water overnight and dried under a stream of N_2. Where severe losses in activity were observed, the films were regenerated by heating under N_2 (10 minutes at 200 ºC, 30 minutes at 300 ºC). Scavenging experiments were carried out on the same 4-chlorophenol solution used in the regular studies, but with the addition of the molecular scavengers (50 mM) tert-butyl alcohol, disodium EDTA, or with constant bubbling of N_2 gas during irradiation. Note: due to interferences between disodium EDTA and 4-chlorophenol in the UV-vis trace, the 4-chlorophenol peak at 280 nm was used to determine the degradation efficiency. Chromium(VI) reduction was carried out in a similar fashion to the degradation of organic pollutants. 2ml of a solution containing Potassium dichromate ($4x10^{-4}$ M) and phenol ($6x10^{-6}$ M) adjusted to pH 1 using H_2SO_4 (4M) was added to a quartz cuvette. A film was then added to the solution and irradiated using the same white LED and filter as was used in the organic photodegradation tests.

Bacterial Strain

The standard *E. coli* ATCC 23716 (American Type Culture Collection, Rockville, MD, USA) were used in this study. The freeze-dried cultures were rehydrated and reactivated according to the manufacturer's instructions. The reactivated *E. coli* were cultured on petri dishes with *Brilliance E. coli/coliform Agar* (Oxoid) selective media using the 'spread plate' technique. The *E. coli* colonies with purple colour appeared on the petri dishes after incubation at 37 °C for 20-24 h. The freshly cultured *E. coli* colonies were used to spike the deionised water (DI) which was sterilised at 121 °C for 15 mints prior to use.

Bacteriacidal Testing

Substrates coated with TiO_2 and C-$TiCl_4$-TiO_2 layers (3.5 × 3.5 cm^2) were each immersed in 50 ml of sterilised DI water spiked with *E.coli* (with initial concentration of 1.2×10^7 CFU/ml, where CFU is colonies forming unit) and illuminated with UV-A lamp. The lamp was placed on top of the water sample at about 8 cm from its surface. An 11W low-pressure blacklight fluorescent lamp (PLS G23, Casell Lighting) emitting predominantly at 365 nm provided UV irradiation. The photon flux emission of the lamp was determined by potassium ferrioxalate actinometer, as described by Murov et al.[87], and found to be 4.98×10^{-6} Einstein/s. At specific time intervals, 2 ml of the water sample were pipetted out and immediately analysed with respect to viable *E. Coli* cells by the serial dilution culture method. For each dilution, 200 µl of the sample were spread on petri dishes with *Brilliance E. coli/coliform Agar* (Oxoid) selective media. The petri dishes were incubated at 37 °C for 20-24 h before viable counts were determined.

References

[1] United Nations Water, *The United Nations World Water Development Report 2016*, **n.d.**

[2] World Health Organisation, *World Health Organisation Water Fact Sheet No. 391*, **2014**.

[3] United Nations, *Water for a Sustainable World*, **2015**.

[4] United Nations Water, *Water Scarcity*, **2013**.

[5] UN Water, *WWAP (United Nations World Water Assessment Programme). 2016. The United Nations World Water Development Report 2016: Water and Jobs*, **2016**.

[6] "United Nations Global Goals," can be found under http://www.globalgoals.org/global-goals/clean-water-sanitation/, **2016**.

[7] J. Machell, K. Prior, R. Allan, J. M. Andresen, *Environ. Sci. Water Res. Technol.* **2015**, *1*, 268–271.

[8] United States Environmental Protection Agency, *National Primary Drinking Water Regulations*, **2016**.

[9] W. Ben, J. Wang, R. Cao, M. Yang, Y. Zhang, Z. Qiang, *Chemosphere* **2017**, *172*, 392–398.

[10] M. K. Ramseier, A. Peter, J. Traber, U. von Gunten, *Water Res.* **2011**, *45*, 2002–2010.

[11] M. Li, C. Wang, M. Yau, J. R. Bolton, Z. Qiang, *Water Res.* **2017**, *108*, 348–355.

[12] A. Benito, A. Penadés, J. L. Lliberia, R. Gonzalez-Olmos, *Chemosphere* **2017**, *166*, 230–237.

[13] Y. Dong, D. Tang, C. Li, *Appl. Surf. Sci.* **2014**, *296*, 1–7.

[14] C. Li, Y. Tang, B. Kang, B. Wang, F. Zhou, Q. Ma, J. Xiao, D. Wang, J. Liang, *Sci. China, Ser. E Technol. Sci.* **2007**, *50*, 279–289.

[15] H. Park, Y. Park, W. Kim, W. Choi, *J. Photochem. Photobiol. C Photochem. Rev.* **2013**, *15*, 1–20.

[16] M. Ge, C. Cao, J. Huang, S. Li, Z. Chen, K.-Q. Zhang, S. S. Al-deyab, Y. Lai, *J. Mater. Chem. A* **2016**, *4*, 6772–6801.

[17] S. Banerjee, S. C. Pillai, P. Falaras, K. E. O'Shea, J. A. Byrne, D. D. Dionysiou, *J. Phys. Chem. Lett.* **2014**, *5*, 2543–2554.

[18] X. Li, H. Lin, X. Chen, H. Niu, J. Liu, T. Zhang, F. Qu, *Phys. Chem. Chem. Phys.* **2016**, *18*, 9176–9185.

[19] L. Zhu, C. Fu Tan, M. Gao, G. W. Ho, *Adv. Mater.* **2015**, *27*, 7713–7719.

[20] S. Li, Z. Zhao, Y. Huang, J. Di, Y. (Alec) Jia, H. Zheng, *J. Mater. Chem. A* **2015**, *3*, 5467–5473.

[21] J. M. Meichtry, I. K. Levy, H. H. Mohamed, R. Dillert, D. W. Bahnemann, M. I. Litter, *ChemPhysChem* **2016**, *17*, 885–892.

[22] L. Fenghui, Y. Jie, T. Guangyuan, Q. Ling, X. Jiacheng, L. Yongdi, L. Wang, L. Juying, J. Zhang, *Appl. Catal. B Environ.* **2017**, *201*, 1–11.

[23] B. A. Marinho, R. O. Cristóvão, R. Djellabi, J. M. Loureiro, R. A. R. Boaventura, V. J. P. Vilar, *Appl. Catal. B Environ.* **2017**, *203*, 18–30.

[24] D. Venieri, A. Fraggedaki, M. Kostadima, E. Chatzisymeon, V. Binas, A. Zachopoulos, G. Kiriakidis, D. Mantzavinos, *Appl. Catal. B Environ.* **2014**, *154–155*, 93–101.

[25] J. J. Murcia, E. G. Ávila-Martínez, H. Rojas, J. A. Navío, M. C. Hidalgo, *Appl. Catal. B Environ.* **2017**, *200*, 469–476.

[26] X. Zeng, Z. Wang, N. Meng, D. T. McCarthy, A. Deletic, J. Pan, X. Zhang, *Appl. Catal. B Environ.* **2017**, *202*, 33–41.

[27] K. Nakata, A. Fujishima, *J. Photochem. Photobiol. C Photochem. Rev.* **2012**, *13*, 169–189.

[28] M. R. Hoffmann, S. T. Martin, W. Choi, D. W. Bahnemann, *Chem. Rev.* **1995**, *95*, 69–96.

[29] X. Chen, S. S. Mao, *Chem. Rev.* **2007**, *107*, 2891–2959.

[30] S. H. Lee, H. Lee, M. Cho, Y. Lee, *Chem. Commun.* **2015**, *51*, 3391–3394.

[31] M. K. Hossain, A. R. Koirala, U. S. Akhtar, M. K. Song, K. B. Yoon, *Chem. Mater.* **2015**, *27*, 6550–6557.

[32] S. Rasalingam, C.-M. Wu, R. T. Koodali, *ACS Appl. Mater. Interfaces* **2015**, *7*, 4368–4380.

[33] W. Zhou, W. Li, J.-Q. Wang, Y. Qu, Y. Yang, Y. Xie, K. Zhang, L. Wang, H. Fu, D. Zhao, *J. Am. Chem. Soc.* **2014**, *136*, 9280–9283.

[34] M. Pelaez, P. Falaras, V. Likodimos, A. G. Kontos, A. A. de la Cruz, K. O'shea, D. D. Dionysiou, *Appl. Catal. B Environ.* **2010**, *99*, 378–387.

[35] H. Zeng, J. Xie, H. Xie, B. Su, M. Wang, H. Ping, W. Wang, H. Wang, Z. Fu, *J. Mater. Chem. A* **2015**, *3*, 19588–19596.

[36] J. Reszczyńska, T. Grzyb, J. W. Sobczak, W. Lisowski, M. Gazda, B. Ohtani, A. Zaleska, *Appl. Catal. B Environ.* **2015**, *163*, 40–49.

[37] J. Zhao, P. Xu, Y. Li, J. Wu, J. Xue, Q. Zhu, X. Lu, W. Ni, *Nanoscale* **2015**, *8*, 5417–5421.

[38] B. Wu, D. Liu, S. Mubeen, T. T. Chuong, M. Moskovits, G. D. Stucky, *J. Am. Chem. Soc.* **2016**, *138*, 1114–1117.

[39] C. T. Dinh, H. Yen, F. Kleitz, T. O. Do, *Angew. Chemie - Int. Ed.* **2014**, *53*, 6618–6623.

[40] J. Pan, X. Li, Q. Zhao, T. Li, M. Tade, S. Liu, *J. Mater. Chem. C* **2015**, *3*, 6025–6034.

[41] Y. Huo, X. Yang, J. Zhu, H. Li, *Appl. Catal. B Environ.* **2011**, *106*, 69–75.

[42] S. J. A. Moniz, J. Tang, *ChemCatChem* **2015**, *7*, 1659–1667.

[43] H. Li, L. Zhou, L. Wang, Y. Liu, J. Lei, J. Zhang, *Phys. Chem. Chem. Phys.* **2015**, *17*, 17406–17412.

[44] Y. Yang, Y. Li, J. Wang, Y. Zhang, D. He, J. Wu, H. Dai, *RSC Adv.* **2015**, *5*, 50833–50842.

[45] Y. Zhang, J. Lu, M. R. Hoffmann, Q. Wang, Y. Cong, Q. Wang, H. Jin, *RSC Adv.* **2015**, *5*, 48983–48991.

[46] L. U. Jefferson, A. D. Netchaev, J. a. Jefcoat, A. D. Windham, F. M. McFarland, S. Guo, R. K. Buchanan, J. P. Buchanan, *ACS Appl. Mater. Interfaces* **2015**, *7*, 12639–12648.

[47] H. Liang, X. Li, *Appl. Catal. B Environ.* **2009**, *86*, 8–17.

[48] N. M. Dimitrijevic, S. Tepavcevic, Y. Liu, T. Rajh, S. C. Silver, D. M. Tiede, *J. Phys. Chem. C* **2013**, *117*, 15540–15544.

[49] Y. Huang, Y. Liang, Y. Rao, D. Zhu, J. Cao, Z. Shen, W. Ho, S. C. Lee, *Environ. Sci. Technol.* **2017**, acs.est.6b04460.

[50] Y. K. Kim, E. B. Kang, S. H. Kim, S. M. Sharker, B. Y. Kong, I. In, K. Lee, S. Y. Park, *ACS Appl. Mater. Interfaces* **2016**, *8*, 29827–29834.

[51] L.-W. Zhang, H.-B. Fu, Y.-F. Zhu, *Adv. Funct. Mater.* **2008**, *18*, 2180–2189.

[52] L. Yu, G. Li, X. Zhang, X. Ba, G. Shi, Y. Li, P. K. Wong, J. C. Yu, Y. Yu, *ACS Catal.* **2016**, *6*, 6444–6454.

[53] P. D. Tran, S. K. Batabyal, S. S. Pramana, J. Barber, L. H. Wong, S. C. J. Loo, *Nanoscale* **2012**, *4*, 3875.

[54] C. Creutz, M. H. Chou, *Inorg. Chem.* **2008**, *47*, 3509–3514.

[55] D. Finkelstein-Shapiro, S. K. Davidowski, P. B. Lee, C. Guo, G. P. Holland, T. Rajh, K. A. Gray, J. L. Yarger, M. Calatayud, *J. Phys. Chem. C* **2016**, *120*, 23625–23630.

[56] B. C. O'Regan, J. R. Durrant, P. M. Sommeling, N. J. Bakker, *J. Phys. Chem. C* **2007**, *111*, 14001–14010.

[57] G. Odling, N. Robertson, *ChemPhysChem* **2017**, *18*, 728–735.

[58] X. K. Wang, C. Wang, W. Q. Jiang, W. L. Guo, J. G. Wang, *Chem. Eng. J.* **2012**, *189–190*, 288–294.

[59] H. Xu, L. Zhang, *J. Phys. Chem. C* **2010**, *114*, 11534–11541.

[60] H. Luo, T. Takata, Y. Lee, J. Zhao, K. Domen, Y. Yan, *Chem. Mater.* **2004**, *16*, 846–849.

[61] W. Zhou, F. Sun, K. Pan, G. Tian, B. Jiang, Z. Ren, C. Tian, H. Fu, *Adv. Funct. Mater.* **2011**, *21*, 1922–1930.

[62] Z. Zhu, Y. Xu, B. Qi, G. Zeng, P. Wu, G. Liu, W. Wang, F. Cui, Y. Sun, *Environ. Sci. Nano* **2017**, *4*, 302–306.

[63] H. Estrade-Szwarckopf, *Carbon N. Y.* **2004**, *42*, 1713–1721.

[64] R. Asahi, T. Morikawa, H. Irie, T. Ohwaki, *Chem. Rev.* **2014**, *114*, 9824–9852.
[65] N. Baram, Y. Ein-Eli, *J. Phys. Chem. C* **2010**, *114*, 9781–9790.
[66] L. N. Quan, Y. H. Jang, K. a Stoerzinger, K. J. May, Y. J. Jang, S. T. Kochuveedu, Y. Shao-Horn, D. H. Kim, *Phys. Chem. Chem. Phys.* **2014**, *16*, 9023.
[67] W. Q. Fang, X. L. Wang, H. Zhang, Y. Jia, Z. Huo, Z. Li, H. Zhao, H. G. Yang, X. Yao, *J. Mater. Chem. A* **2014**, *2*, 3513.
[68] L. Samiolo, M. Valigi, D. Gazzoli, R. Amadelli, *Electrochim. Acta* **2010**, *55*, 7788–7795.
[69] A. Mills, J. Wang, D. F. Ollis, *J. Phys. Chem. B* **2006**, *110*, 14386–14390.
[70] U. G. Akpan, B. H. Hameed, *J. Hazard. Mater.* **2009**, *170*, 520–529.
[71] I. K. Konstantinou, T. A. Albanis, *Appl. Catal. B Environ.* **2004**, *49*, 1–14.
[72] G. Odling, N. Robertson, *ChemPhysChem* **2016**, *17*, 2872–2880.
[73] D. Hou, X. Hu, P. Hu, W. Zhang, M. Zhang, Y. Huang, *Nanoscale* **2013**, *5*, 9764.
[74] M. Rico-Santacruz, Á. E. Sepúlveda, E. Serrano, E. Lalinde, J. R. Berenguer, J. García-Martínez, *J. Mater. Chem. C* **2014**, *2*, 9497–9504.
[75] M. Stylidi, D. I. Kondarides, X. E. Verykios, *Appl. Catal. B Environ.* **2004**, *47*, 189–201.
[76] W. Shan, Y. Hu, Z. Bai, M. Zheng, C. Wei, *Appl. Catal. B Environ.* **2016**, *188*, 1–12.
[77] L. Chen, M. Chen, D. Jiang, J. Xie, *J. Mol. Catal. A Chem.* **2016**, *425*, 174–182.
[78] L. Yu, X. Zhang, G. Li, Y. Cao, Y. Shao, D. Li, *Appl. Catal. B Environ.* **2016**, *187*, 301–309.
[79] R. Sedghi, F. Heidari, *RSC Adv.* **2016**, *6*, 49459–49468.
[80] World Health Organisation, *Guidelines for Drinking-Water Quality - Second Edition - Volume 2 - Health Criteria and Other Supporting Information - Addendum*, **1998**.
[81] O. Carp, C. L. Huisman, A. Reller, *Prog. Solid State Chem.* **2004**, *32*, 33–177.
[82] J. Marugán, R. van Grieken, C. Sordo, C. Cruz, *Appl. Catal. B Environ.* **2008**, *82*, 27–36.
[83] M. Janus, A. Markowska-Szczupak, E. Kusiak-Nejman, A. W. Morawski, *Environ. Prot. Eng.* **2012**, *38*, 89–97.
[84] W. C. Oh, A. R. Jung, W. B. Ko, *Mater. Sci. Eng. C* **2009**, *29*, 1338–1347.
[85] O. Akhavan, M. Abdolahad, Y. Abdi, S. Mohajerzadeh, *Carbon N. Y.* **2009**, *47*, 3280–3287.
[86] O. Akhavan, R. Azimirad, S. Safa, M. M. Larijani, *J. Mater. Chem.* **2010**, *20*, 7386–7392.
[87] S. L. Murov, I. Carmichael, G. L. Hug, *Handbook of Photochemistry, Second Edition*, **1993**.

Acknowledgements

The authors would like to thank the CRITICAT Centre for Doctoral Training (Ph.D. studentship to O.G.; grant code: EP/L016419/1) and EPSRC GCRF (grand code: EP/P510944/1) for financial support. X-ray photoelectron spectra were obtained at the National EPSRC XPS Users' Service (NEXUS) at Newcastle University, an EPSRC Mid-Range Facility. Open data: http://dx.doi.org/10.7488/ds/2070

Keywords: Photocatalysis • Water Purification • Carbon layer • Cl-doping • Bacteria